pH-Controlled Assembly and Disassembly of Electrostatically Linked CdSe−SiO_2 and Au−SiO_2 Nanoparticle Clusters

Hiroki Hiramatsu and Frank E. Osterloh*

Department of Chemistry, University of California at Davis, Davis, California 95616

Received February 7, 2003. In Final Form: May 8, 2003

The effect of pH on the self-assembly and disassembly of nanoparticle aggregates (clusters) of amine modified silica spheres (50 nm) and carboxylic acid modified gold (7 nm) or cadmium selenide (6 nm) spheres was investigated using electron microscopy and infrared and electronic spectroscopy. 4-Mercaptobenzoic acid (MBA) ligated cadmium selenide nanoparticles were synthesized by ligand exchange on 6 nm trioctylphosphine oxide ligated CdSe nanoparticles in basic methanol solution at room temperature. Reaction of CdSe(MBA) and 11-mercaptoundecanoic acid (MUA) ligated gold nanoparticles with tetramethylammonium hydroxide in methanol or THF produced CdSe$(MBA)^-[N(CH_3)_4^+]$ and Au$(MUA)^-$-$[N(CH_3)_4^+]$ as black solids. On the basis of signal integration in the ^1H NMR spectra, organic groups occupy areas of 0.44 nm^2 (MBA), 0.22 nm^2 (MUA), and 0.69 nm^2 (APS) on the nanoparticle surfaces. Combination of these modified colloids with solutions of 3-aminopropylsiloxane ligated colloidal silica in aqueous solution at various pHs yielded core−shell type clusters in which the smaller gold or cadmium selenide spheres are bound to the surfaces of the larger silicate spheres. In the pH interval from 6.8 to 11.1, the Au/CdSe nanocrystal content of the clusters was found to be inversely related to the pH. The addition of a 50 mM Na_3PO_4/H_3PO_4 buffer solution attenuated the pH dependence of composition in the case of the SiO_2@Au clusters, due to screening of the surface potential of the charged particles by ions of opposite charge. Whereas in neutral water the nanoparticle clusters are inert toward rearrangement and decomposition, at pH > 13, rapid disassembly of the clusters occurs as a consequence of deprotonation of the primary ammonium groups. The stability of the clusters is accurately described with a semiquantitative electrostatic binding model, in which the bond strength between nanoparticles is determined by their surface charge concentrations. These surface charge concentrations are calculated from the Henderson−Hasselbach equation using estimated and measured pK_a values for 4-mercaptobenzoic acid (4.79), 3-aminopropylsilane (9.27), and MUA (5.7) monolayers.

Introduction

Inorganic nanoparticles are attractive building blocks for the construction of nanostructured materials and devices with adjustable physical and chemical properties.[1,2] With a variety of inorganic nanoparticles now at hand,[3−6] the identification of chemical methods for the selective linkage of these nano building blocks to produce nanostructured aggregates, or clusters, of controllable structure becomes increasingly important. Bond types employed for this purpose can be classified as electrostatic,[7,8] covalent,[9−11] van der Waals,[12] coordinative,[13−15] hydrogen-bond-like,[16,17] and magnetostatic.[18] Combinations of different bond types are present in nanoparticle clusters, that are supported by either antibody−antigene interactions,[19,20] complementary DNA strand dimerization,[21,22] or cyclodextrine-based host−guest interactions.[23] Additional bond types have been utilized.[24−26]

The nature of the bonding between nanoparticles determines stability and dynamics of a nanoparticle cluster and its collective physical properties (by mediating electronic and magnetic coupling between nanoparticles). The ability to adjust the strength and nature of the bonds

* To whom correspondence should be addressed. E-mail: fosterloh@ucdavis.edu.

(1) Fendler, J. H. *Nanoparticles and Nanostructured Films*: *Preparation, Characterization and Applications*; Wiley-VCH: Weinheim, 1998.
(2) Kamat, P. V.; Meisel, D. *Semiconductor Nanoclusters*: *Physical, Chemical, and Catalytic Aspects*; Elsevier: Amsterdam, 1997.
(3) Murray, C. B.; Kagan, C. R.; Bawendi, M. G. *Annu. Rev. Mater. Sci.* **2000**, *30*, 545−610.
(4) Sugimoto, T. *Fine particles*: *synthesis, characterization, and mechanisms of growth*; Marcel Dekker: New York, 2000.
(5) Johnson, B. F. G. *Coord. Chem. Rev.* **1999**, *192*, 1269−1285.
(6) Collier, C. P.; Vossmeyer, T.; Heath, J. R. *Annu. Rev. Phys. Chem.* **1998**, *49*, 371−404.
(7) Galow, T. H.; Boal, A. K.; Rotello, V. M. *Adv. Mater.* **2000**, *12*, 576−579.
(8) Mayya, K. S.; Gittins, D. I.; Caruso, F. *Chem. Mater.* **2001**, *13*, 3833−3836, 7A.
(9) Musick, M. D.; Keating, C. D.; Lyon, L. A.; Botsko, S. L.; Pena, D. J.; Holliway, W. D.; McEvoy, T. M.; Richardson, J. N.; Natan, M. J. *Chem. Mater.* **2000**, *12*, 2869−2881.
(10) Brust, M.; Bethell, D.; Kiely, C. J.; Schiffrin, D. J. *Langmuir* **1998**, *14*, 5425−5429.
(11) Gomez, S.; Erades, L.; Philippot, K.; Chaudret, B.; Colliere, V.; Balmes, O.; Bovin, J. O. *Chem. Commun.* **2001**, 1474−1475.
(12) Fendler, J. H. *Chem. Mater.* **1996**, *8*, 1616−1624.
(13) Wuelfing, W. P.; Zamborini, F. P.; Templeton, A. C.; Wen, X. G.; Yoon, H.; Murray, R. W. *Chem. Mater.* **2001**, *13*, 87−95.
(14) Kim, Y. J.; Johnson, R. C.; Hupp, J. T. *Nano Lett.* **2001**, *1*, 165−167.
(15) Cumberland, S. L.; Berrettini, M. G.; Javier, A.; Strouse, G. F. *Chem. Mater.* **2003**, *15*, 1047−1056.
(16) Boal, A. K.; Rotello, V. M. *Langmuir* **2000**, *16*, 9527−9532.
(17) Boal, A. K.; Ilhan, F.; DeRouchey, J. E.; Thurn-Albrecht, T.; Russell, T. P.; Rotello, V. M. *Nature* **2000**, *404*, 746−748.
(18) Puntes, V. F.; Krishnan, K. M.; Alivisatos, A. P. *Science* **2001**, *291*, 2115−2117.
(19) Shenton, W.; Davis, S. A.; Mann, S. *Adv. Mater.* **1999**, *11*, 449−452, 427.
(20) Sapp, S. A.; Mitchell, D. T.; Martin, C. R. *Chem. Mater.* **1999**, *11*, 1183−1185, 5A.
(21) Loweth, C. J.; Caldwell, W. B.; Peng, X. G.; Alivisatos, A. P.; Schultz, P. G. *Angew. Chem., Int. Ed.* **1999**, *38*, 1808−1812.
(22) Mirkin, C. A. *Inorg. Chem.* **2000**, *39*, 2258−2272.
(23) Liu, J.; Mendoza, S.; Roman, E.; Lynn, M. J.; Xu, R. L.; Kaifer, A. E. *J. Am. Chem. Soc.* **1999**, *121*, 4304−4305.
(24) Brust, M.; Kiely, C. J.; Bethell, D.; Schiffrin, D. J. *J. Am. Chem. Soc.* **1998**, *120*, 12367−12368.
(25) Marinakos, S. M.; Brousseau, L. C.; Jones, A.; Feldheim, D. L. *Chem. Mater.* **1998**, *10*, 1214−1219.
(26) Lim, M. H.; Ast, D. G. *Adv. Mater.* **2001**, *13*, 718−721.

10.1021/la034217t CCC: $25.00
Published on Web 07/03/2003

between nanoparticles is thus a key factor in building structures with specified functions, such as chemical sensors, switches, and motors. A better understanding of the bonds in nanoparticle clusters will also lead to advanced synthetic methods for the manipulation and derivatization of individual nanoparticles. Reversibly attachable colloidal particles could, for example, be employed as protecting groups for other nanoparticles and thus allow their regio-selective chemical modification.

To better understand and control the bonding in electrostatically linked nanoparticle clusters, we undertook a systematic investigation of the aggregation of aryl- and alkylcarboxylic acid modified 7 nm gold and 6 nm CdSe nanoparticles with 3-aminopropylsilyl modified silica nanoparticles. The organic groups on the surface of these particles are ionized in water due to acid−base reactions with the solvent. When aqueous solutions of complementary particles are combined, core−shell type SiO_2@Au and SiO_2@CdSe nanoparticle clusters form, whose structures and stabilities are sensitive functions of solution pH and electrolyte concentration. Variation of the pH not only allows one to control the structure of the formed clusters, but also to initiate their disassembly. The dependence of cluster composition and stability on pH can be rationalized with a simple electrostatic model, that calculates the cluster stability as a function of the surface charge densities of the linked nanoparticles. These densities are calculated from the Henderson−Hasselbach equation using estimated and measured pK_a values for the immobilized organic acids.

Experimental Section

11-Mercaptoundecanoic acid (MUA, Aldrich), 4-mercaptobenzoic acid (MBA, Aldrich), 3-aminopropyltrimethoxysilane (APS, Aldrich), concentrated ammonium hydroxide solution (Acros), and absolute ethanol (Gold Shield Chemical Co.), were used as received. All operations in aqueous environments were conducted using ultrapure water with a resistance greater than 18 MΩ. Reactions that involved photosensitive CdSe colloids were performed in dimmed light. Trioctylphosphine oxide (TOPO) ligated CdSe particles (6 nm) were synthesized using Peng's method.[27] pH values were measured with a AgCl/KCl glass electrode attached to a pH meter (Accumet AB15, Fisher Scientific). Prior to the measurements, the pH electrode was calibrated using a buffer solution at pH = 4 (sodium biphthalate), 7 (potassium phosphate), and 10 (potassium bicarbonate). Separations were performed on a Fisher Marathon model 21000 centrifuge with a fixed angle rotor (13 750 rpm = 21 000*g*). Electron microscopy measurements were performed on FEI XL30-SFEG scanning electron and Philips CM-12 transmission electron microscopes, under 10 kV (scanning electron microscopy (SEM)) and 100 kV (transmission electron microscopy (TEM)) operating voltages, respectively. Samples for imaging were deposited either onto holey carbon TEM grids (Ted Pella) or onto unmodified silicon wafers or aluminum stubs. IR spectra were recorded on KBr pellets using a Mattson Galaxy Series FTIR 3000 IR spectrometer. UV/vis spectra were recorded on samples dispersed in water on a Hewlett-Packard 8450A spectrometer. ^{1}H NMR spectra were recorded in deuterated water on a Mercury 300 MHz NMR spectrometer. Spectra were calibrated to the solvent signals.

Synthesis of 50 nm SiO_2·($SiCH_2CH_2CH_2NH_2$)·HCl. Particles were synthesized using a modification of the published Stoeber synthesis.[28] Tetraethyl orthosilicate (3.8 mL, 5.3 g, 25 mmol) was added to a mixture of 5.7 mL of concentrated aqueous ammonium hydroxide and 114 mL of ethanol with stirring. The slightly opaque solution was stirred overnight. A 50 mL aliquot of the resulting SiO_2 colloidal dispersion was removed and used for further reactions: 1.0 mL (1.4 g, 7.9 mmol) of 3-aminopropyltrimethoxysilane was quickly added with stirring. The solution was left to stir overnight during which the opaqueness of the solution increased noticeably. The colloidal silica was isolated by centrifugation at 13 750 rpm and washed with three portions of 50 mL of ethanol. After the washing, a positive ninhydrin test confirmed the presence of organic amines. The precipitate was dispersed in 50 mL of tetrahydrofuran, and 0.1 M HCl was slowly added to precipitate the amine-functionalized silica as a hydrochloride. The addition was stopped when no more precipitate formed. The precipitate was collected by centrifugation at 3600 rpm and dried under a vacuum to afford a white powder of amine-functionalized colloidal silica. The dried powder is soluble in water to give clear solutions of the functionalized silica. Product identity was confirmed by scanning electron microscopy and ^{1}H/^{13}C NMR (D_2O).

Synthesis of Au·[$S(CH_2)_{10}CO_2^-$][$N(CH_3)_4$]$^+$. A modified version of the published procedure was employed.[29] Tetrachloroauric acid (68 mg, 0.2 mmol) was dissolved in 10 mL of water, and the resulting solution was then added to the stirred solution of tetraoctylammonium bromide (437 mg, 0.800 mmol) in 100 mL of toluene. Within 5 min of rapid stirring, the yellow color of the tetrachloroaurate completely transferred to the toluene phase. After 25 min, a freshly prepared sodium tetrahydroborate (76 mg, 2.0 mmol) solution in 10 mL of water was added to the rapidly stirred biphasic mixture, causing a sudden color change from orange to gray and then to bright red. The solution was left to stir for another hour. The toluene phase containing the gold colloid was then separated from the water phase and washed three times with water to extract excess ions. 11-Mercaptoundecanoic acid (500 mg) dissolved in ∼20 mL of toluene was then added in three portions, which resulted in complete precipitation of the colloid. The black precipitate was collected by centrifugation and washed with 50 mL of toluene three times to remove excess thiol. The precipitate was then dispersed in tetrahydrofuran and precipitated again by adding several drops of tetramethylammonium hydroxide (20 wt % in methanol). The resulting precipitate was centrifuged off, washed three times with 40 mL portions of ethanol, and dried in vacuo to afford 45 mg of the carboxylate-functionalized gold colloid. This solid was soluble in water. The solid was characterized by scanning electron microscopy, ^{1}H NMR, and IR and UV/vis spectroscopy.

Synthesis of CdSe·(4-$SC_6H_4CO_2^-$)[$N(CH_3)_4^+$]. To 300 mg of TOPO ligated CdSe particles was added a large excess (400 mg, 2.6 mmol) of 4-mercaptobenzoic acid dissolved in 15 mL of methanol. The resulting mixture was ultrasonicated for 1 h. To this dispersion was added dropwise a 20 wt % solution of tetramethylammonium hydroxide in methanol (approximately 1.5 g of the solution), until the precipitate had dissolved completely to give a dark brown solution, which was stored in the dark for 1 h. Twenty-five milliliters of 20% hexane in tetrahydrofuran was added to precipitate the functionalized CdSe nanoparticles. The precipitate was washed three times with 40 mL portions of 5% methanol in tetrahydrofuran, and the brown solid was collected and dried in vacuo. The ligated CdSe nanoparticles (6 nm) are soluble in H_2O and methanol. Product identity was confirmed by ^{1}H NMR (D_2O), IR spectroscopy, and SEM.

Synthesis of CdSe−SiO_2 Composites. Composites were synthesized at four different pH conditions by combining the respective nanoparticles as solutions in aqueous ammonium hydroxide. For example, 1.0 mg of 6 nm CdSe·(4-$SC_6H_4CO_2^-$)-[$N(CH_3)_4^+$] was dissolved in 2.0 mL of the 0.1 M ammonium hydroxide solution, and in a separate vial 1.5 mg of SiO_2 was dissolved in 1.0 mL of an 0.1 M ammonium hydroxide solution. The silica dispersion was then added quickly to the ultrasonicated solution of CdSe nanoparticles, and the mixture was left under sonication for 5 min, after which the pH was determined using a pH meter. The solids were isolated by centrifugation at 10 000 rpm and washed with 3.0 mL of the 0.1 M ammonia solution. These steps were repeated three to four times in order to remove excess CdSe nanoparticles from the composite. The resultant solid was dispersed in 3.0 mL of water. TEM samples were prepared by immersion of a holey carbon copper grid in the

(27) Aldana, J.; Wang, Y. A.; Peng, X. *J. Am. Chem. Soc.* **2001**, *123*, 8844−8850.

(28) Stoeber, W.; Fink, A.; Bohn, E. *J. Colloid Interface Sci.* **1968**, *26*, 62−69.

(29) Brust, M.; Walker, M.; Bethell, D.; Schiffrin, D. J.; Whyman, R. *J. Chem. Soc., Chem. Commun.* **1994**, 801−802.

Scheme 1. Surface Derivatization of Au, CdSe, and SiO_2 Nanoparticles with Organosilanes and Alkane- and Arenethiols

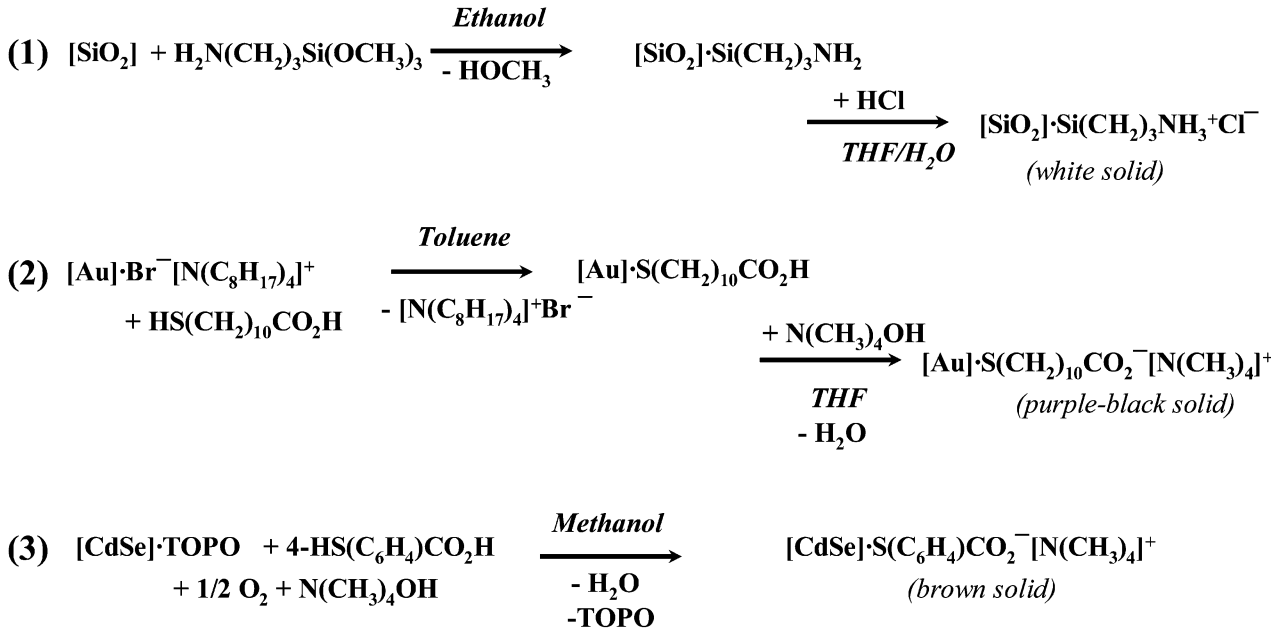

Table 1. Conditions Employed for the Synthesis of Nanoparticle Clusters

sample	CdSe [mg]	Au [mg]	total volume [mL]	NH_4OH [mol L^{-1}]	measured pH
A	1.0		3.0	0	8.4
B	1.0		3.0	0.0001	8.6
C	1.0		3.0	0.01	10.2
D	1.0		3.0	0.1	11.1
A′		3.0	10.0	0	6.8
B′		3.0	10.0	0.0001	7.2
C′		3.0	10.0	0.01	10.2
D′		3.0	10.0	0.1	11.1

solution for 1 h, followed by drying in vacuo overnight. UV−vis spectra were recorded from these dispersions. Other composites were synthesized using nanoparticle and ammonia solutions with the concentrations listed in Table 1.

Synthesis of Au−SiO_2 Composites. The syntheses were carried out as described for CdSe−SiO_2, except that more solvent was used. For example, a solution of 3.0 mg of the 7 nm gold nanoparticles in 9.0 mL of 0.1 M aqueous NH_3 was added to a solution of 1.5 mg of SiO_2 in 1.0 mL of 0.1 M NH_3. The mixture was ultrasonicated for 5 min, and after measurement of the pH, the solid was isolated by centrifugation at 10 000 rpm. The solid was dispersed in 10.0 mL of the ammonia solution and centrifuged off again. These washing steps were carried out three to four times, after which the resultant composite was dispersed in 10.0 mL of water for further analysis. UV−vis spectra were recorded on these dispersions without further dilution. TEM samples were prepared as described above. Table 1 lists the specific amounts and concentrations used for syntheses at different pHs.

In a separate experiment, several SiO_2@Au composites were assembled at five pH conditions (4.9, 6.5, 7.8, 8.7, and 9.6) using 50 mM buffer solutions (phosphate for pH 4.9−7.8, tris(hydroxymethyl)aminomethane for pH 8.7, and sodium carbonate for pH 9.6). In the general procedure, 3.0 mL of H_2O was mixed with 1.0 mL of buffer and 2.0 mL of gold colloid solution ($\sim 3.9 \times 10^{14}$ particles/mL) was then added. To this mixture, 0.10 mL of a silica nanoparticle stock solution (0.5 mg/mL; $\sim 2.2 \times 10^{12}$ particles/mL) was added followed by sonication for 10 min. The mixture was kept for 24 h, after which time the composite was separated by centrifugation at 8000 rpm and washed with 30 mL of buffer solution ($\sim$5 mM). The resulting precipitate was suspended in 12 mL of water, which contained 3 mL of the 50 mM buffer solution. Samples from the suspensions were characterized by SEM.

Reaction of SiO_2@Au and SiO_2@CdSe Composites with 50 nm SiO_2·($SiCH_2CH_2NH_2$)·HCl. A 0.5 mL portion of the Au−SiO_2 (sample A′) or CdSe−SiO_2 (sample A) composite dispersion was diluted to 1.0 mL with water, and 1.5 mg of amine-functionalized silica nanoparticles in 1.0 mL of water was added. The mixture was ultrasonicated for at least 2 h and then centrifuged at 3600 rpm to afford a solid and a colorless supernatant. The solid was redispersed in 2.0 mL of water, and a sample was deposited onto a silicon substrate for SEM.

Reaction of SiO_2@Au and SiO_2@CdSe Composites with NMe_4OH. To 0.5 mL of the SiO_2@Au and SiO_2@CdSe composite dispersions, respectively, was added three drops of 20 wt % NMe_4OH in methanol with stirring. The mixture with the SiO_2@Au turned bright red immediately. The dispersions were ultrasonicated for 1 h and then centrifuged to afford a red supernatant and a precipitate noticeably lighter in color in the case of the SiO_2@Au composite. For the SiO_2@CdSe composite, a brown supernatant and a light brown precipitate formed. The precipitates were washed twice with 5.0 mL portions of water and redispersed in 2.0 mL of water. Samples for SEM were obtained from these dispersions.

Results and Discussion

Carboxylic acid and alkylamine modified Au, CdSe, and SiO_2 nanoparticles were obtained according to reactions 1−3 in Scheme 1.

Reaction of 3-aminopropyltrimethoxysilane with 50 nm silicate nanoparticles according to a modified version of the published Stoeber[28] procedure yielded silica nanoparticles terminated on their surface with primary amines. Subsequent treatment with hydrochloric acid in THF produced the hydrochloride salt of the colloid, which could be isolated as a white powder and redispersed in water to give optically clear solutions.

Reaction of alkylammonium-protected gold nanoparticles (7 nm) with 11-mercaptoundecanoic acid according to a modified version of the published Brust method[29] yielded particles with surface-immobilized carboxylic acid residues. To obtain a water-soluble material, the acid ligated gold particles were converted into the tetramethylammonium salt, by reaction with tetramethylammonium hydroxide in THF/ethanol. This afforded a black precipitate, which was dried in vacuo.

For the first time, 4-mercaptobenzoic acid was employed as a ligand for cadmium selenide particles that were

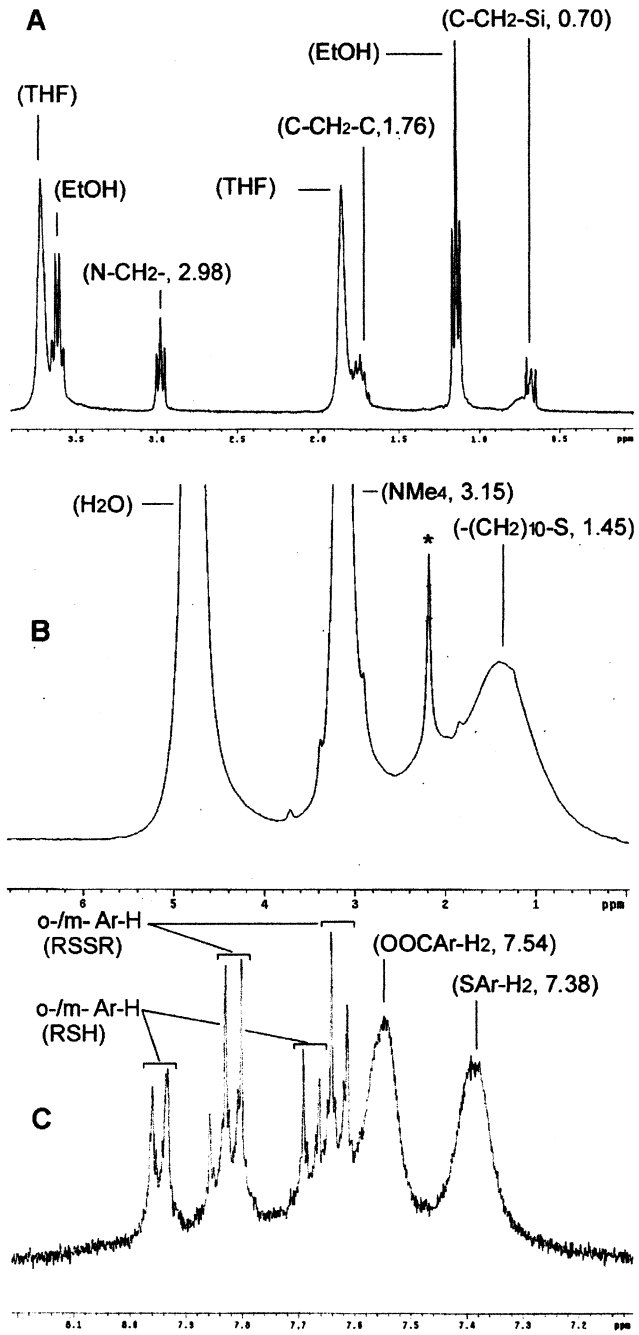

Figure 1. ^{1}H NMR spectra (300 MHz) of (A) SiO_2·APS$^+$Cl$^-$, (B) Au·MUA$^-$[$(NCH_3)_4$]$^+$, and (C) CdSe·MBA$^-$[$(NCH_3)_4$]$^+$ (all in D_2O). (*) Acetone impurity.

obtained according to Peng's method.[27] Ligand exchange of trioctylphosphine oxide by the aromatic thiol in methanol required the addition of excess base, which was provided in the form of tetramethylammonium hydroxide. After sonication and stirring at room temperature for 1 h, selective precipitation of the thiol ligated nanoparticles by a THF/hexane mixture and drying *in vacuo* afforded a black solid of the tetramethylammonium salt. In agreement with its ionic nature, this salt is freely soluble in water and alcohols, slightly in THF, but not in nonpolar hydrocarbons.

^{1}H NMR spectra (Figure 1) recorded for solutions of the modified nanoparticles confirmed binding of the organic ligands. Based on signal integration, it was possible to quantitate the number of ligands on the nanoparticle surfaces.

The spectrum of the SiO_2·APS nanoparticles (A) in water shows signals for all protons from the 3-aminopropylene portion of the ligand. The narrow width of these signals is somewhat surprising for a nanoparticle of this large size (50 nm). Usually the proton signals of nanoparticle-bound ligands are broadened by dipolar coupling effects, especially when the nanoparticles are larger than 5−10 nm.[30] The absence of this broadening indicates either a low ligand surface concentration and/or a porous surface structure that leads to disorder among organic ligands on the surface. A porous structure would also explain the ability of the colloid to absorb ethanol and THF. Traces of these solvents (visible in the NMR) could not be removed from the silica nanoparticles despite drying in vacuo overnight.

All protons of the 11-mercaptoundecanoic acid ligands in the spectrum (B) of the Au·MUA$^-$[$(NCH_3)_4$]$^+$ could be accounted for. The methylene peaks are quite broad and appear as a very broad single peak spanning from 0.5 to 2.5 ppm. The countercation is observable at its usual position as an intense singlet at 3.15 ppm.

The spectrum of CdSe·MBA$^-$[$(NCH_3)_4$]$^+$ nanoparticles (C) contains two broad singlets at 7.38 and 7.54 ppm of *o*- and *m*-arene protons of the bound thiol. Two sets of sharp peaks reveal the presence of both unbound 4-mercaptobenzoic acid and its oxidation product bis(4-carboxyphenyl)disulfide. The free thiol appears to be in equilibrium with its bound form. It is presently not clear whether the disulfide forms by oxidation of the free thiol or by photooxidation of bound thiol. The latter process has been previously described.[31,32] To minimize photooxidation, CdSe particles were manipulated in subdued light.

The number of ligands on the surface of the nanoparticles and their packing areas were obtained by comparing the proton signal intensities of MUA, MBA, and APS ligands and [$N(CH_3)_4$]$^+$ countercations in the ^{1}H NMR spectra of the respective colloids in D_2O with an added dimethyl sulfoxide (DMSO) standard of known concentration. DMSO was chosen because of its miscibility with water and because its proton signal at 2.71 ppm does not overlap with ligand signals. The calculation (full details are given in the Supporting Information) yielded the following values: 258 ligands per particle (MBA), 698 ligands per particle (MUA), and 11 700 ligands per particle (SiO_2) (values for MBA and MUA were obtained by averaging signal intensities of countercations and ligands), which translates into 0.44 nm^2 (MBA), 0.22 nm^2 (MUA), and 0.69 nm^2 (APS) for the corresponding ligand packing areas. The value for MUA is in excellent agreement with that obtained for a mercaptoundecanoic acid self-assembled monolayer (SAM) on gold (0.226 nm^2).[33] The observed value of 0.44 nm^2 for MBA on CdSe is very reasonable, if one considers that 50% of the surface sites are blocked by selenide. Boerio et al. determined the packing area of 3-aminopropylsilane molecules in a SAM on a SiO_2 surface as 0.4 nm^2.[34] Our value of 0.69 nm^2 corresponds to a 40% smaller packing density of ligands on SiO_2 nanoparticles. This is of course possible, because the reaction of 3-aminopropyltrimethoxysilane with the SiO_2 colloid was performed under nonoptimized conditions.

(30) Ingram, R. S.; Hostetler, M. J.; Murray, R. W. *J. Am. Chem. Soc.* **1997**, *119*, 9175−9178.
(31) Aldana, J.; Wang, Y. A.; Peng, X. G. *J. Am. Chem. Soc.* **2001**, *123*, 8844−8850.
(32) Veinot, J. G. C.; Galloro, J.; Pugliese, L.; Pestrin, R.; Pietro, W. J. *Chem. Mater.* **1999**, *11*, 642−648.
(33) Tamada, K.; Ishida, T.; Knoll, W.; Fukushima, H.; Colorado, R.; Graupe, M.; Shmakova, O. E.; Lee, T. R. *Langmuir* **2001**, *17*, 1913−1921.
(34) Boerio, F. J.; Armogan, L.; Cheng, S. Y. **1980**, *73*, 416.

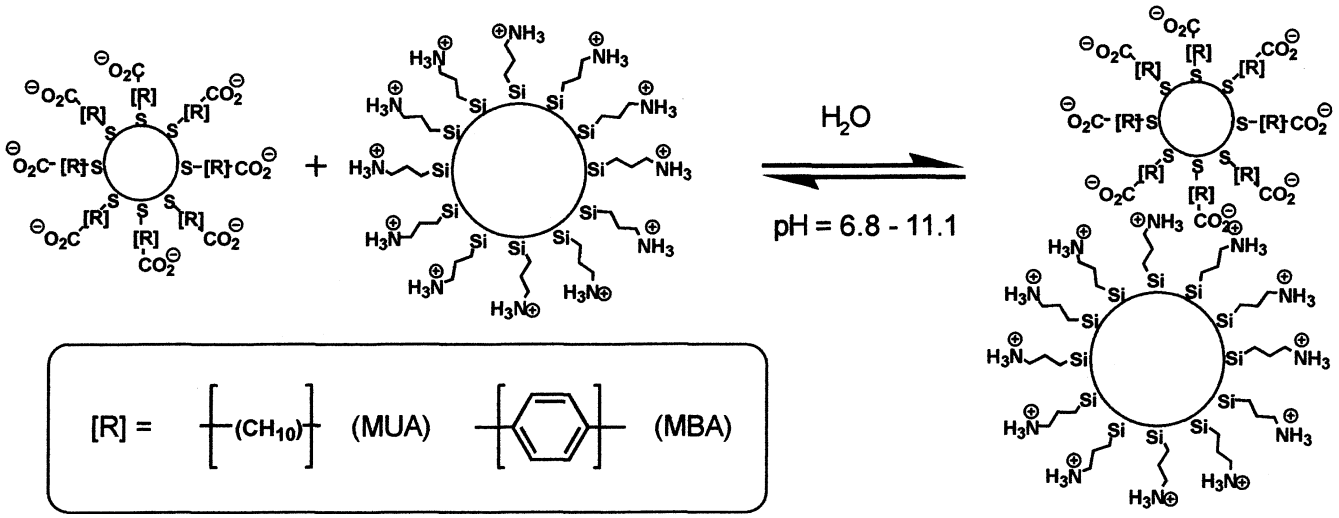

Figure 2. Synthesis of the nanoparticle composites. Drawn not to scale. Countercations/-anions are omitted. The pH was adjusted with aqueous NH_3. Forces between particles with opposite charges are attractive; forces between particles with same charges are repulsive.

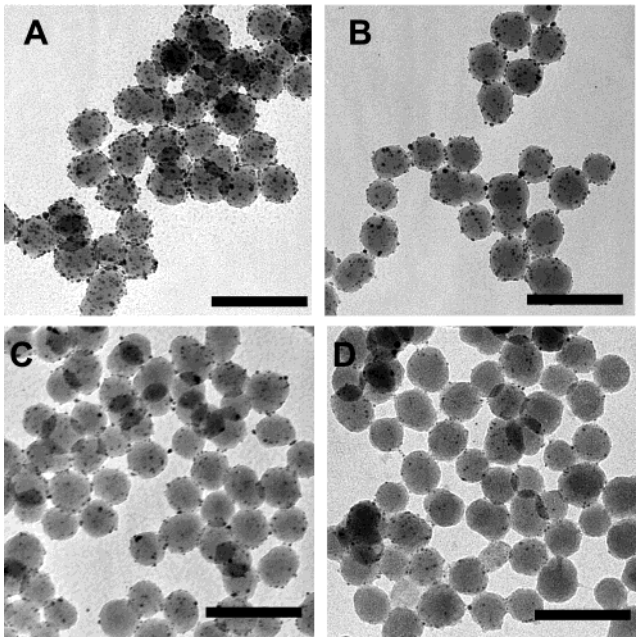

Figure 3. Transmission electron micrographs of SiO_2@Au nanoparticle clusters synthesized at pH = 8.4 (A), 8.6 (B), 10.2 (C), and 11.1 (D). The scale bar for all micrographs is 200 nm.

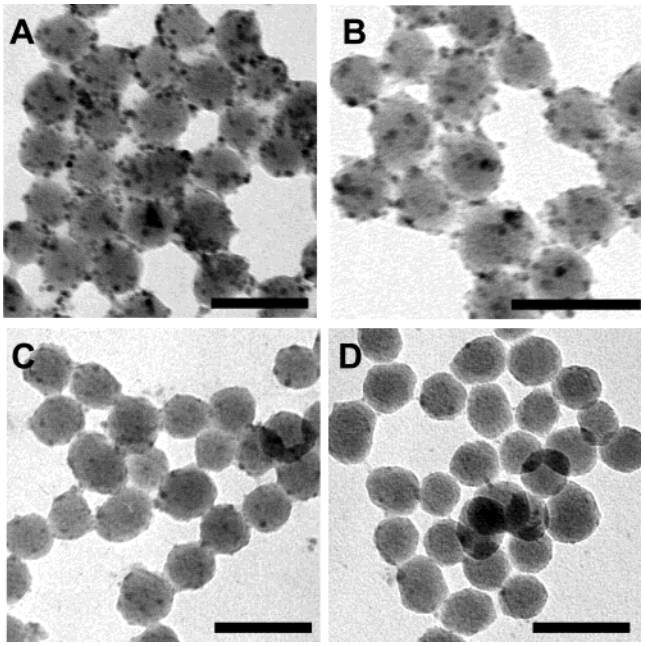

Figure 4. Transmission electron micrographs of SiO_2@CdSe nanoparticle clusters synthesized at pH = 6.8 (A), 7.2 (B), 10.2 (C), and 11.1 (D). Scale bars are 100 nm.

Ligand modified 50 nm SiO_2, 7 nm Au, and 6 nm CdSe nanoparticles were employed for the electrostatic assembly of core−shell type clusters. This was accomplished by combining pH-adjusted solutions of either gold or cadmium selenide particles with pH-adjusted solutions of aminopropyl modified silica colloids (Figure 2). The ratio of gold (CdSe) particles to silica particles was at least 100:1 in order to ensure that the composition of the formed clusters was not limited by the reaction stoichiometry. The mixtures were ultrasonicated for 5 min at room temperature, and the clusters were then collected by centrifugation (10 000 rpm) as pale to deep red (SiO_2@Au) and pale to deep brown (SiO_2@CdSe) solids.

Transmission electron micrographs of SiO_2@Au and SiO_2@CdSe composites formed at the indicated solution pH values are shown in Figures 3 and 4. Both types of composites consist of discrete clusters whose cores are composed of silica spheres to which Au and CdSe nanoparticles are attached. The resulting structures resemble the Au−SiO_2, Ag−SiO_2, and Ag−polystyrene composites prepared by Halas et al.,[35,36] Dong et al.,[37] and Wei et al.,[38] although the particles in our study are much smaller. The distribution of the smaller nanocrystals over the silica surface is quite homogeneous, although at higher coverage direct Au−Au and CdSe−CdSe interactions can also be observed. This is particularly obvious for the SiO_2@CdSe composite assembled at low pH. In the remaining composites, the separation between surface-immobilized Au/CdSe nanocrystals is likely due to coulomb repulsion effects between negatively charged carboxylate ligated nanocrystals. Similar effects between Au nanoparticles

(35) Westcott, S. L.; Oldenburg, S. J.; Lee, T. R.; Halas, N. J. *Langmuir* **1998**, *14*, 5396−5401.
(36) Jackson, J. B.; Halas, N. J. *J. Phys. Chem. B* **2001**, *105*, 2743−2746.
(37) Dong, A. G.; Wang, Y. J.; Tang, Y.; Ren, N.; Yang, W. L.; Gao, Z. *Chem. Commun.* **2002**, 350−351.
(38) Sadtler, B.; Wei, A. *Chem. Commun.* **2002**, 1604−1605.

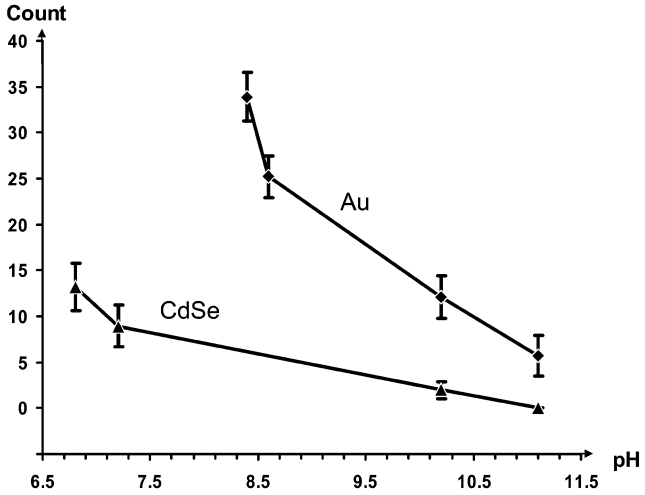

Figure 5. Plot of the Au/SiO_2 (diamonds) and CdSe/SiO_2 ratio (triangles) for composites assembled at different pH values, based on optical analysis of 40 (SiO_2@Au) and 80 (CdSe@SiO_2) randomly selected nanoparticle clusters.

in self-assembled films have been previously observed by the groups of Natan[39] and Johnson.[40]

In Figure 5, the numbers of gold and CdSe nanoparticles per silica sphere are plotted as a function of the pH. Despite relatively large standard deviations in individual data points, a trend of increasing gold/CdSe coverage with decreasing pH is obvious. The smallest quantities of Au/CdSe nanoparticles were assembled on the surface of silica at pH = 11.1. As the solution becomes more acidic, a growing number of Au (CdSe) particles bind to the surfaces of the silica particles, with the highest coverage being achieved at pH = 6.8 for CdSe (13) and 8.4 for Au (33). If the pH is reduced further, the formation of core−shell type clusters abruptly ceases and Au and CdSe nanoparticles begin to flocculate. This is shown for Au nanoparticles in Figure 6A. As the theoretical analysis (see below) will show, the reason for the flocculation is that at pH < 7.5 repulsive electrostatic interactions between Au·MUA^- nanoparticles are replaced by attractive hydrogen-bond and van der Waals interactions.

The selectivity of the nanoparticle assembly is markedly attenuated by electrolytes in the reaction mixture. SiO_2@Au composites synthesized in the pH interval from 6.5 to 8.7 in the presence of a 50 mmol/L H_3PO_4/Na_3PO_4 buffer have nearly identical compositions (the pH 7.8 sample is shown in Figure 6B; for others see the Supporting Information).

SiO_2@Au and SiO_2@CdSe nanoparticle clusters assembled in the absence of electrolytes are remarkably stable against disassembly and rearrangement in aqueous solution. When an aqueous mixture of SiO_2@Au and fresh SiO_2·NH_2 particles is ultrasonicated for 2 h at room temperature, no transfer of Au from the composite onto SiO_2·NH_2 occurs and physical mixtures of the unchanged starting materials are obtained after the treatment (Figure 6C). SiO_2@CdSe composites show a similar inertness against CdSe exchange (Figure 6D). This has preparative importance, because it allows a washing of the core−shell type composites with neutral water without affecting their composition. Unreacted starting materials can thus be conveniently removed.

Table 2. Selected IR Bands [cm^{-1}] and Assignments (Samples as KBr Pellets)

CdSe[a]	SiO_2·CdSe[a]	assignment
3013		C−H of $N(CH_3)_4^+$
1666	1629	H−O
1585		C═O
1488		C−H of $N(CH_3)_4^+$
	1097	Si−O
1012, 842, 783		1,4-disubstituted arenes
949		C−H of $N(CH_3)_4^+$

Au[a]	SiO_2·Au[a]	assignment
3020		C−H of $N(CH_3)_4^+$
2918	2920	C−H
2848	2850	C−H
1728	1709	C═O of CO_2H
	1631	
1564	1564	C═O of CO_2^-
1487		C−H of $N(CH_3)_4^+$
	1093	Si−O
957		C−H of $N(CH_3)_4^+$

SiO_2[a]	assignment
3130−3030	NH_3^+
2900	C−H
1630	H−O of bound water
1102	Si−O

[a] All spectra show broad bands at 3700−2800 cm^{-1} for coordinated water.

In alkaline environments, the composites show drastically reduced stability. Immediate disassembly of the SiO_2@Au composites occurs when the pH of the solution is adjusted to >13 with tetramethylammonium hydroxide. Solids collected after the reactions contain gold and SiO_2 particles as separate units (Figure 6E). In the system SiO_2@CdSe/$Me_4N(OH)$, the disassembly occurs at pH > 11. A comparison of the sample shown in Figure 6F with that in Figure 4A shows the number of silica-bound CdSe particles is greatly reduced, although some residual CdSe nanocrystals are present. The amount of nonremovable CdSe increased in aged samples of the SiO_2@CdSe composites, which might be due to a transition of the bonding from electrostatic to covalent.

Spectroscopic Properties

UV/vis and IR spectra of the pure nanoparticles and their composites prepared at different pH values are shown in Figures 7−9; important band positions and their assignments are listed in Table 2.

Electronic spectra of the pure gold nanoparticles (Figure 7A) are dominated by the gold surface plasmon band at 518 nm. This band is unchanged in the composite with low gold content but shifts to 522 nm as the Au nanoparticle packing density increases. In the limit of complete aggregation of Au·MUA^- particles (in solutions at pH < 7.0), the plasmon band is shifted to 550 nm. As the particle−particle distance is shortest in these closely packed Au nanoparticle clusters, dipolar coupling between gold nanoparticles is maximized.[3,41]

In contrast to the SiO_2@Au clusters, the SiO_2@CdSe clusters do not show any qualitative changes of the electronic spectra as a function of composition. In all spectra (Figure 8), the absorption edge at 640 nm (caused by the lowest energy band gap transition of the nanoparticles) is preserved, albeit with increasing extinction as the CdSe content increases. The associated band gap

(39) Grabar, K. C.; Smith, P. C.; Musick, M. D.; Davis, J. A.; Walter, D. G.; Jackson, M. A.; Guthrie, A. P.; Natan, M. J. *J. Am. Chem. Soc.* **1996**, *118*, 1148−1153.

(40) Sato, T.; Brown, D.; Johnson, B. F. G. *Chem. Commun.* **1997**, 1007−1008.

(41) Lazarides, A. A.; Kelly, K. L.; Jensen, T. R.; Schatz, G. C. *THEOCHEM−J. Mol. Struct.* **2000**, *529*, 59−63.

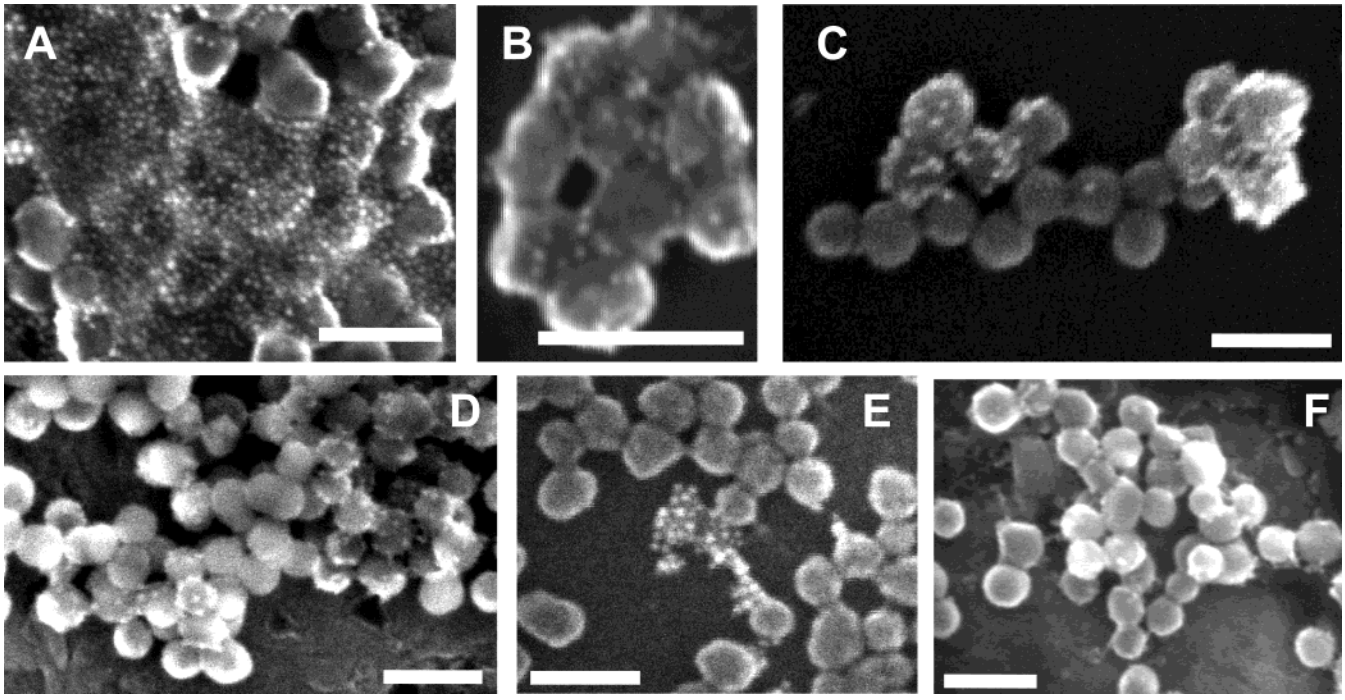

Figure 6. Scanning electron micrographs of (A) SiO_2@Au composite assembled at pH = 4.9, (B) SiO_2@Au composite assembled at pH = 7.8 in the presence of 50 mmol/L H_3PO_4/Na_3PO_4 buffer, (C) SiO_2@Au after treatment with SiO_2·APS^+Cl^-, (D) SiO_2@CdSe after treatment with SiO_2·APS^+Cl^-, (E) SiO_2@Au after reaction with $[N(CH_3)_4]OH$ in water, and (F) SiO_2@CdSe (sample A in Figure 4) after reaction with $[N(CH_3)_4]OH$ in water. All scale bars are 100 nm.

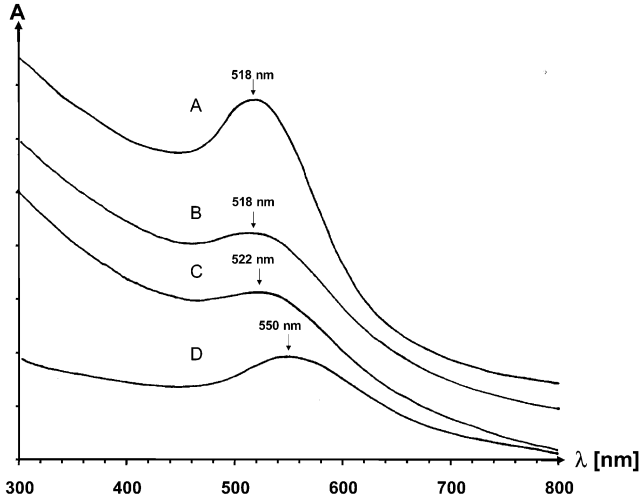

Figure 7. UV−vis spectra of (a) Au·$MUA^-[N(CH_3)_4]^+$, (b) SiO_2@Au composites (pH = 10.2), (c) SiO_2@Au composites (pH = 8.4), and (d) aggregated Au·MUA nanoparticles (pH = 4.9). All spectra were recorded in water.

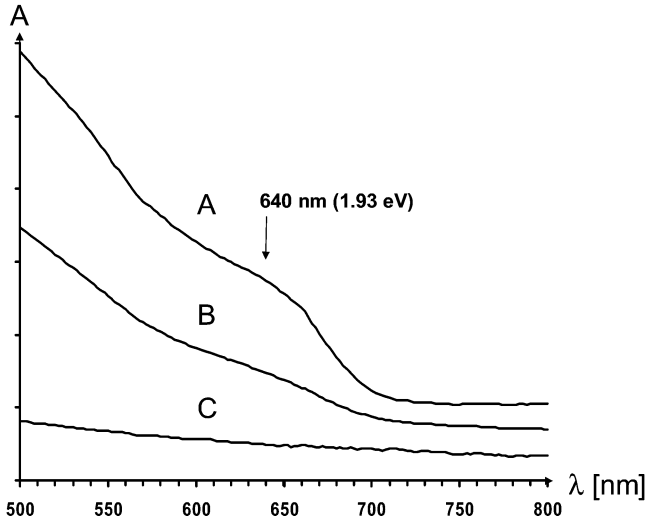

Figure 8. UV−vis spectra of (A) CdSe·$MBA^-[N(CH_3)_4]^+$, (B) SiO_2@CdSe nanoparticle cluster (pH = 6.8), and (C) SiO_2·APS^+Cl^- (all recorded in water).

of 1.933 eV of this transition corresponds to a mean nanoparticle diameter of 7 nm,[42] which slightly exceeds the value of 6 nm as determined by TEM.

IR spectra of the ligand modified nanoparticles and their composites are in agreement with the expected compositions. The spectrum of the SiO_2·$(CH_2)_3NH_3Cl$ colloid (Figure 9C) is dominated by a strong Si−O band at 1102 cm^{-1} and bands at 3300 and 1630 cm^{-1} for coordinated water. The aliphatic APS ligands give rise to a weak C−H band at 2900 cm^{-1}, whereas the NH_3^+ groups lead to a broad absorption at 3130−3030 cm^{-1}. While the ligands in the Au·MUA^- particles (spectrum A) lead to aliphatic stretching vibrations at 3020 and 2918 cm^{-1} and 2850 cm^{-1}, respectively, the bands of the Ar−H vibrations in CdSe·MBA^- are too weak to be observed (spectrum B). However, the presence of a characteristic band pattern in the fingerprint region (ring vibration) reveals the presence of the 1,4-disubstituted phenyl groups. For both Au·MUA^- and CdSe·MBA^- particles, C=O bands shifted to 1564 and 1585 cm^{-1} clearly show that the carboxylic acid functions are deprotonated. The negative charge of the ligands is balanced by the $N(CH_3)_4^+$ cations, which have three characteristic bands at 3013, 1488, and 949 cm^{-1} in the case of CdSe. These bands vanish upon formation of the SiO_2@Au and SiO_2@CdSe clusters (spectra D and E), demonstrating the expected loss of the $N(CH_3)_4^+$ cations. The strong C−H bands of the MUA ligands are still visible in the spectrum of the SiO_2@Au composite, while the bands of the MBA ligands are no longer observed in the

(42) Norris, D. J.; Bawendi, M. G. *Phys. Rev. B* **1996**, *53*, 16338−16346.

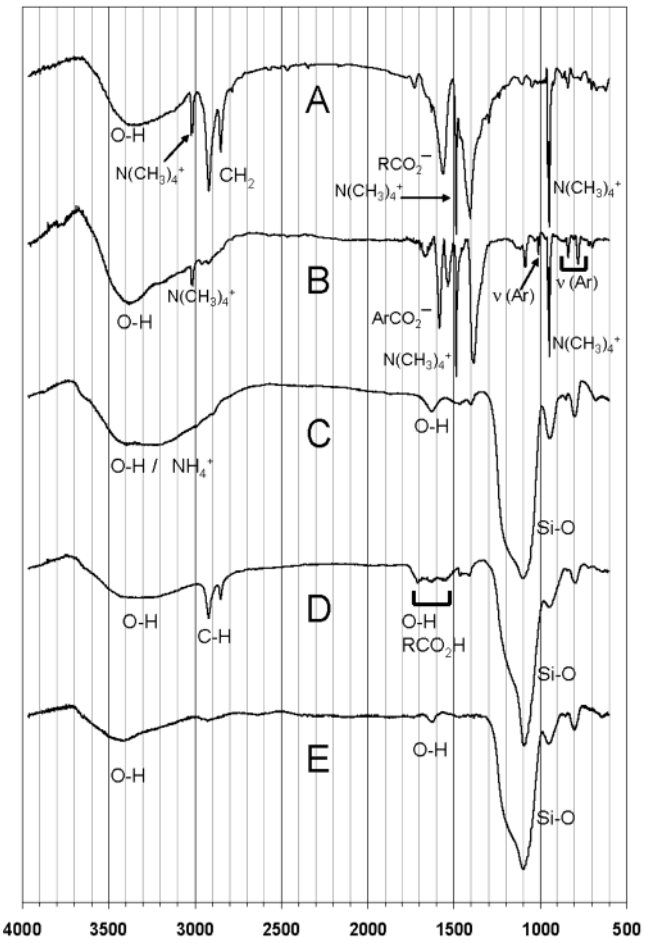

Figure 9. IR spectra of (A) Au·MUA$^-$[N(CH$_3$)$_4$]$^+$, (B) CdSe·MBA$^-$[N(CH$_3$)$_4$]$^+$, (C) SiO$_2$·APS$^+$Cl$^-$, (D) SiO$_2$@Au composite (pH = 8.4), and (E) SiO$_2$@CdSe composite (pH = 6.8). All samples were prepared as KBr pellets. Wavenumbers are given in Table 2.

SiO$_2$@CdSe composite due to the lower thiol surface concentration as compared to Au (see below). In the case of the SiO$_2$@Au composite, a set of weak bands can be discerned at 1709, 1631, and 1564 cm^{-1}, which are assigned to coordinated water and to MUA in both protonated and deprotonated forms. The presence of a mixture of MUA·H$^+$ and MUA·$^-$ is expected considering the high pK_a of the surface-immobilized acid (5.7).

Analysis and Discussion

The pH-dependent self-assembly of SiO$_2$@Au and SiO$_2$@CdSe nanoclusters in aqueous solution can be described with a simple electrostatic binding model which correlates the binding strength between nanoparticles with their pH-dependent surface charge density. For the calculation of the latter, the packing densities σ of the organic ligands on the nanoparticle surfaces are considered together with their degree of ionization. Assuming one positive or negative charge per residue, Au, CdSe, and SiO$_2$ particles obtain surface charge densities σ of −0.70, −0.35, and 0.40 C m^{-2}, respectively. Here, σ is calculated as the product of packing density [molecules/m^2] and charge of the electron [1.602 × 10^{-19} C]. The actual charge densities are lower because, depending on pH, only a fraction x_i of the residues are charged. This fraction can be calculated from the Henderson−Hasselbach equation using slightly adjusted pK_a values of the respective acidic/basic residues. The pH-dependent surface charge density σ for SiO$_2$ particles is

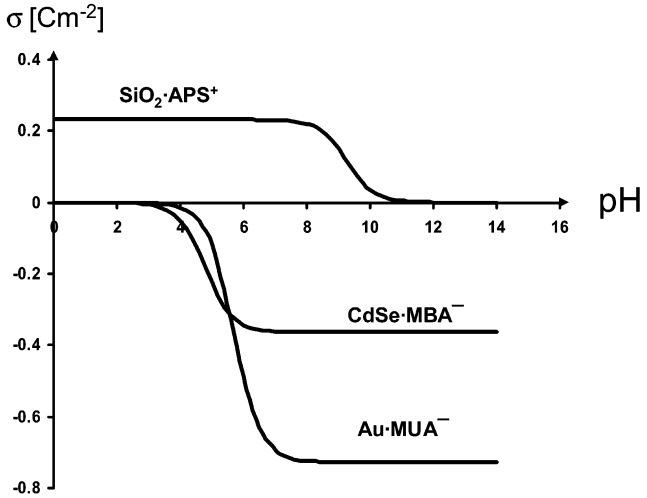

Figure 10. Calculated positive and negative surface charge densities for silica·APS$^+$, Au·MUA$^-$, and CdSe·MBA$^-$ as a function of the pH. The value for Au·MUA$^-$ is about twice as negative as that of CdSe·MBA$^-$ because of the higher thiol surface density.

$$\sigma_{SiO_2} = \sigma_{0,SiO_2} x_{RNH_3^+} = \sigma_{0,SiO_2} \frac{10^{pK_a(RNH_3^+)-pH}}{10^{pK_a(RNH_3^+)-pH} + 1} \quad (1)$$

For Au and CdSe particles,

$$\sigma_{Au} = \sigma_{0,Au} x_{RCO_2^-} = \sigma_{0,Au} \frac{10^{pH-pK_a(RCO_2H)}}{10^{pH-pK_a(RCO_2H)} + 1} \quad (2)$$

The pK_a is equal to 5.7 for surface-absorbed MUA and was previously measured using electrode capacitance.[43] The values for MBA and APS were estimated from *p*-chlorobenzoic acid (3.98)[44] and propylammonium (10.71).[44] The actual values used for the calculation (4.79 for MBA and 9.27 for APS) reflect further corrections for electrostatic effects that are expected between charged groups in densely packed monolayers (electrostatic repulsion between charged residues leads to an acidity reduction for MBA and to an acidity increase for APS·H$^+$).[45] Surface charge densities calculated on the basis of these pK_a values are plotted for Au, CdSe, and SiO$_2$ particles as functions of the solution pH in Figure 10.

Appreciable charge densities are generated at pH > 4 in the case of the acid modified particles and at pHs smaller than 10 for the base modified silica particles. The charge densities are positive for alkylammonium-coated SiO$_2$ and negative for carboxylate-coated Au and CdSe particles. From the charge densities, the bond strength between two oppositely charged nanoparticles can be approximated with eq 3, which describes the electrostatic energy W_{EL} between two point charges at the distance R_{12}. Since the most important electrostatic interactions between two nanoparticles are expected to occur at their common interfaces, the charges q_1 and q_2 in eq 3 are simply determined as products of the contact areas (estimated as

(43) Smalley, J. F.; Chalfant, K.; Feldberg, S. W.; Nahir, T. M.; Bowden, E. F. *J. Phys. Chem. B* **1999**, *103*, 1676−1685.

(44) Weast, R. C. *CRC Handbook of Chemistry and Physics*, 1st student ed.; CRC Press: Boca Raton, FL, 1988.

(45) For silica-bound APS, the pK_a of the conjugate acid is estimated by reducing the pK_a for propylamine (10.71) (ref 43) by 1.44. This is based on the observation that in 1,4-diaminobutane the pK_a of the second protonation equilibrium (9.71) is by 1.44 lower than the pK_a of the first (11.15) because of electrostatic repulsion. The pK_a of the MBA monolayer is increased by 0.81, because the pK_a of a MUA monolayer (5.7) (ref 42) is by 0.81 units higher than that of free octanoic acid (4.89) (ref 43).

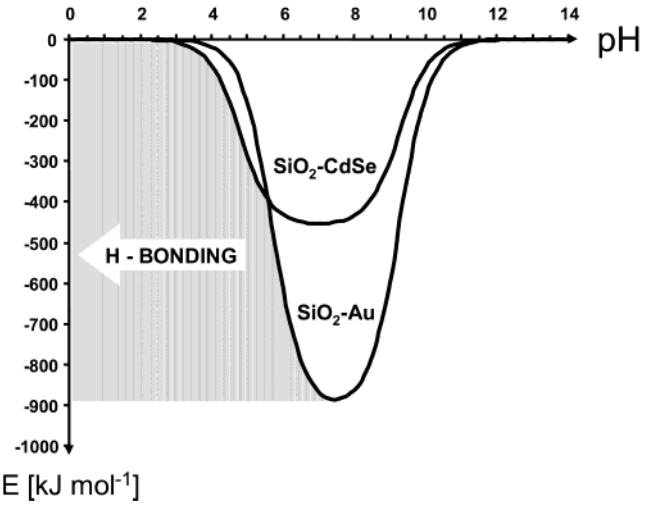

Figure 11. Calculated electrostatic energies [kJ per mole] for SiO_2−Au and SiO_2−CdSe nanoparticle dimers as a function of the pH. The energies were calculated from eq 3 with R_{12} = 1 nm, $\epsilon_r = 81.1$ for water, and A_1,$A_2 = 9$ nm^2 and with charge densities from eqs 1 and 2.

$A_1 = A_2 = 9$ nm^2) and their respective charge densities σ. With $R_{12} = 1$ nm as the average distance between the charged organic groups and with $\epsilon_r(H_2O) = 81.1$, one obtains $W_{EL} \approx -10^3$ kJ per mole of particle dimers (-10^{-18} J per particle dimer), which is in satisfactory agreement with more advanced Derjaguin−Landau−Verwey−Overbeek (DLVO) calculations for related systems (6×10^{-19} J).[46]

$$W_{EL} = \frac{q_1 q_2}{4\epsilon_0 \epsilon_r \pi R_{12}} = \frac{\sigma_1 A_1 \sigma_2 A_2}{4\epsilon_0 \epsilon_r \pi R_{12}} \qquad (3)$$

In Figure 11, the electrostatic energies for pairs SiO_2−CdSe and SiO_2−Au are plotted as a function of pH. The strongest electrostatic interactions occur at pH = 7 for the SiO_2@CdSe and at pH = 7.5 for the SiO_2@Au clusters. At smaller or greater pH values, the electrostatic interactions are reduced due to partial protonation of carboxylates (pH < 6) or partial deprotonation of ammonium groups (pH > 8). Over the entire pH range, the electrostatic energy of the CdSe−SiO_2 composites is smaller than for the Au−SiO_2 composite, because of the lower surface concentration of ionizable groups on the CdSe nanocrystals. In addition, electrostatic interactions between SiO_2−CdSe are reduced because the smaller CdSe nanoparticles have a greater curvature, and their contact area is thus smaller than that of Au particles (CdSe = 6 nm, Au = 7 nm). This size effect was not considered in the calculation.

The predicted magnitudes of electrostatic interaction are in good agreement with the experimental data (plots in Figure 5). No formation of core−shell type clusters takes place at pH > 11, because the amine residues on the Au and CdSe particles are fully deprotonated and positive charge and the electrostatic energy are essentially zero. As the pH is lowered from 11 to 6.8, the number of Au and CdSe in the composites does increase. However, with the decrease of negative charge on the acid modified nanoparticles the selectivity of the assembly deteriorates, illustrated by an increasing percentage of direct CdSe−CdSe contacts in the SiO_2@CdSe composites. As repulsive interactions between carboxylate ligated nanoparticles are reduced, attractive van der Waals forces and hydrogen bonding between RCO_2H groups begin to dominate. This explains why maximum Au−SiO_2 bonding occurs at pH = 8.4 and not at pH = 7.5 as predicted by the purely electrostatic model. At pH < 6.8 (CdSe·MBA) and pH < 7.5 (Au·MUA), assembly of core−shell type clusters stops entirely, and flocculates of Cd·MBA and Au·MUA form instead. Partial flocculation is already observed at (<8.4 for Au·MUA).

The electrostatic model also explains the reduced stability of CdSe/Au−SiO_2 nanoparticle clusters in the presence of a buffer solution. Electrolytes screen the surface charges of the colloidal particles by forming a diffuse double layer of ions of opposite charges around the nanoparticles. According to Debye−Hueckel theory, the thickness of this layer (as defined by 1/e decrease of the surface potential) decreases with the inverse square root of the ionic strength of the solution.[47] The addition of 50 mM Na_3PO_4/H_3PO_4 to a solution of the nanoparticles and 4 mM NH_4OH leads to a reduction of the double-layer thickness from ~5 to 0.7 nm. This value is below the length of a 11-mercaptoundecanoic acid molecule (~1.2 nm) and comparable to the length of 4-mercaptobenzoic acid (0.7 nm). The electric fields of the ionizable groups are thus strongly attenuated by the ions, and electrostatic bonding is suppressed. This explains the lower pH dependence of Au−SiO_2 cluster formation in this case.

Conclusions

In conclusion, we have shown that amine modified SiO_2 and carboxylic acid modified Au and CdSe nanoparticles self-assemble in aqueous solution to give well-defined core−shell type clusters, whose composition can be controlled with the pH. In neutral water, the clusters are stable toward disassembly and rearrangement. In an alkaline environment with pH > 13, the composites undergo rapid disassembly into the separate nanoparticles. The influence of pH on composition and stability of the nanoclusters can be understoood in terms of a simple electrostatic model, which calculates stability as a function of the electrostatic energy between ionizable surface groups. The pH dependence of the surface charge of the nanoparticles is accurately described using pK_a values for the free acids which had to be slightly adjusted for electrostatic effects.

Acknowledgment. We thank Professor Thorsten Dieckmann and his group for the pH meter. This work was supported by start-up funds of the University of California at Davis and by a type G award (No. 38057-G5) of the Petroleum Research Fund administered by the American Chemical Society.

Supporting Information Available: Electron micrographs of SiO_2@Au composites assembled in the presence of a buffer solution, surface charge densities and electrostatic energies calculated with eqs 1−3, and experimental details of the optical particle analysis. This material is available free of charge via the Internet at http://pubs.acs.org.

LA034217T

(46) Evans, D. F.; Wennerström, H. *The Colloidal Domain*: *Where Physics, Chemistry, Biology, and Technology Meet*, 2nd ed.; Wiley-VCH: New York, 1999; p 413.

(47) Myers, D. *Surfaces, Interfaces, and Colloids*: *Principles and Applications*; VCH: New York, 1991; p 75.